SAND2022-4061C

Design and Testing of Discriminants for Local Seismic Events Recorded During the Redmond Salt Mine Monitoring Experiment in Utah

Rigobert Tibi[1], Nathan Downey[1], and Ronald Brogan[2]

[1)] Sandia National Laboratories; [2)] ENSCO, Inc., Melbourne, FL

Email: rtibi@sandia.gov

INTRODUCTION

The Redmond Salt Mine Monitoring Experiment in Utah was designed to record seismoacoustic data at distances less than 50 km for algorithm testing and development. During the experiment from October 2017 to July 2019, six broadband seismic stations were operating at a time, with three of them having fixed locations for the duration, while the three other stations were moved to different locations every one-and-half to two-and-half months. Redmond Salt Mine operations consist of night-time underground blasting several times per week. These blasts occur in a large underground tunnel complex, tens of miles long. Redmond Mine is located within a belt of active seismicity, allowing for easy comparison of natural and anthropogenic sources.

THE REDMOND SALT MINE MONITORING EXPERIMENT

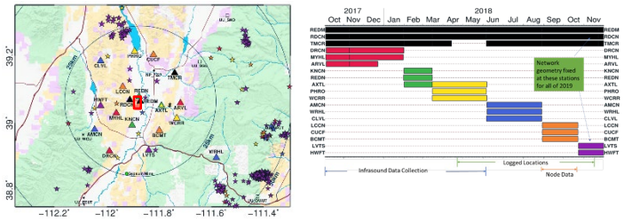

Fig. 1. (Left) Locations (triangles) of broadband stations for the Redmond Mine Experiment. The red box outlines the Redmond Mine area. (Right) Operational timeline of the stations.

DATA

Using the recorded dataset, we built 1373 events with local magnitude (M_L) of −2.4 and lower to 3.3. For 284 of the events, both M_L and the coda duration magnitude (M_C) are well constrained (see Fig. 2 below). Based on the event locations and the signal onset characters, this subset was divided into three populations:

- 75 blasts from the Redmond Salt Mine (**RMEs**),
- 206 tectonic earthquakes (**EQs**), and
- 3 blasts (**QBs**) from a mine/quarry located about 8 km from the Redmond Salt Mine.

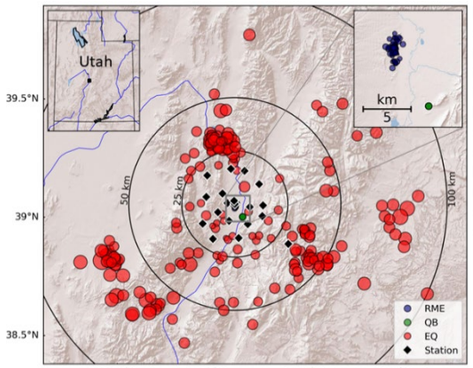

Fig. 2. Locations (circles) of the 284 events from the subset. The size of the circle is proportional to the event magnitude. Red symbols represent earthquakes (EQs), navy circles in the inset the Redmond mine events (RMEs), and green circles in the inset the quarry blasts (QBs).

We used the subset of events to design and test discriminants that are effective at local distances.

MAGNITUDE-BASED DISCRIMINATION

- For M_L calculation, the mean peak *Sg* amplitudes were estimated from the horizontal components after conversion to displacement as would be measured by a Wood-Anderson seismometer; and the empirical distance corrections were estimated according to Pechmann et al. (2007).
- M_C was calculated according to the procedure described in Pechmann et al. (2006), using the equation for the Utah region proposed by these authors.

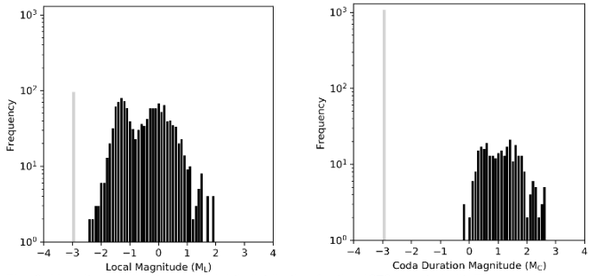

Fig. 3. Magnitude (M_L left and M_C right) distribution for the 1373 events built. The gray bar in each plot represents the number of events for which the magnitude could not be estimated.

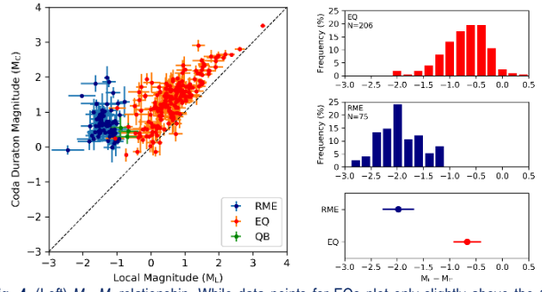

Fig. 4. (Left) M_L–M_C relationship. While data points for EQs plot only slightly above the 1:1 line (dashed line), data points for the mining events (RMEs & QBs) are significantly off that line. This results from enhanced coda for the shallow mining events (Koper et al., 2016). (Right) Distribution and median of M_L–M_C for the EQ and RME populations. Chi-square tests suggest that the two populations are statistically distinct.

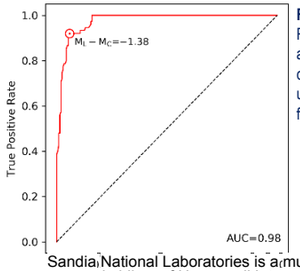

Fig. 5. ROC curve for a binary classifier between RMEs and EQs. The optimum M_L–M_C cutoff associated with the closest point to the ideal classifier is −1.38. The high value for the area under the curve (AUC=0.98) is a clear indication for a very effective discriminant.

DISCRIMINATION BASED ON FREQUENCY CONTENTS

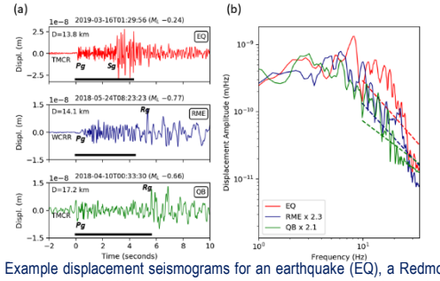

Fig. 6. (a) Example displacement seismograms for an earthquake (EQ), a Redmond Mine event (RME), and a quarry blast (QB). Visible phases are labeled. (b) Spectra for the seismograms shown in (a). The dashed lines are regression lines for the frequency range from 10 to 35 Hz. The steeper fall-off slope for the EQ indicates a lack of high-frequency energy. This constitutes the basis for the discriminant based on *Sg* low-to-high frequency ratio.

Measurement of Sg Amplitudes

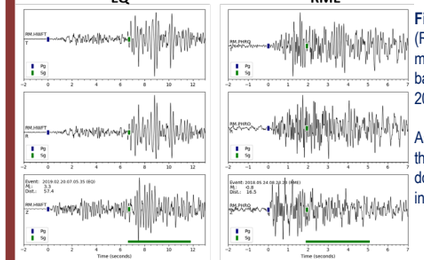

Fig. 7. The root mean square (RMS) of the *Sg* amplitudes are measured in the three frequency bands 10–15 Hz, 15–20 Hz, and 20–30Hz.

As a result of the Parseval's theorem, the RMS in the time domain is equivalent to the RMS in the frequency domain.

Separation of Source Excitation, Propagation, and Site Terms

- The recorded amplitude A_{ij} for an event *i* recorded at a station *j* is expressed as in Equation 1.

$$\log A_{ij}(f) = \log EXC_i(f) + \log SITE_j(f) + \log G(r_{ij}, f) \quad (1)$$

  $EXC_i(f)$: Source excitation term for source *i*; $SITE_j(f)$: Site term for station *j*; $G(r_{ij}, f)$: Distance-correction term (combined effect of geometrical spreading and attenuation); r_{ij}: Distance from source *i* to station *j*.
- We parameterized the distance-correction term using a piecewise linear function (Yazd, 1993; Kintner et al., 2020). We defined series of nodes, r_k, in 5-km increment over the source-distance range of 5–100 km ($k = 1, 2, \ldots, 20$).
- Distance-correction term, $G(r_{ij}, f)$, approximated using linear interpolation:

$$G(r_{ij}, f) = G(r_k, f) + \frac{(r_{ij} - r_k)}{(r_{k+1} - r_k)}\left(G(r_{k+1}, f) - G(r_k, f)\right) \quad (2)$$

- Linearized equation for an observation at r_{ij} between r_k and r_{k+1}:

$$\log A_{ij}(f) = \log EXC_i(f) + \log SITE_j(f) + q\log G(r_k, f) + p\log G(r_{k+1}, f), \quad (3)$$

  where $p = \frac{(r_{ij} - r_k)}{(r_{k+1} - r_k)}$ and $q = 1 - p$
- Matrix form: $\boldsymbol{a} = \boldsymbol{Jm}$ (4)
  - $\boldsymbol{a}$: Array of logarithm of amplitude measurements
  - $\boldsymbol{m}$: Array of logarithm of model parameters (source excitation terms, station site terms, and distance-correction terms at nodes 5, 10, 15, …, 100 km)
    - 276 sources, 19 stations, and 20 distance nodes.
- Constraint: For r_k= 5 km, $G(r_k, f) = 1/r_k$ (i.e., only geometrical spreading, no attenuation) (5)

DISCRIMINATION BASED ON FREQUENCY CONTENTS (CONT'D)

Site and Distance-Correction Terms

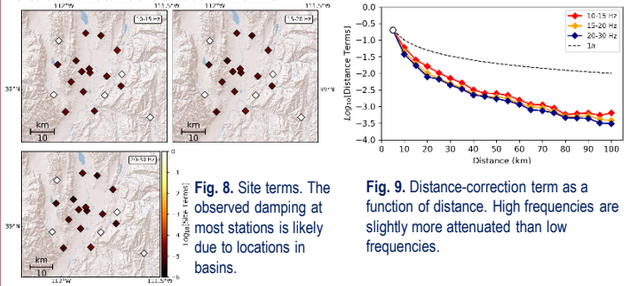

Fig. 8. Site terms. The observed damping at most stations is likely due to locations in basins.

Fig. 9. Distance-correction term as a function of distance. High frequencies are slightly more attenuated than low frequencies.

Source Terms and Discrimination Based on Sg Low-to-High Frequency Ratio

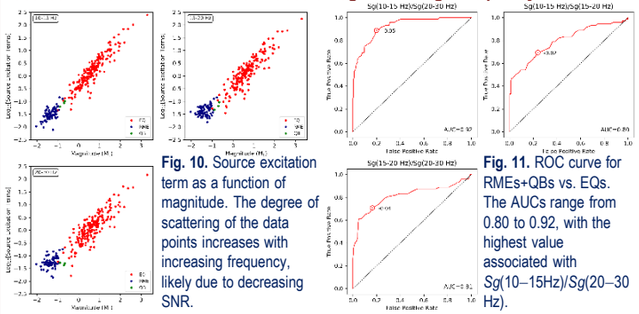

Fig. 10. Source excitation term as a function of magnitude. The degree of scattering of the data points increases with increasing frequency, likely due to decreasing SNR.

Fig. 11. ROC curve for RMEs+QBs vs. EQs. The AUCs range from 0.80 to 0.92, with the highest value associated with *Sg*(10–15Hz)/*Sg*(20–30 Hz).

CONCLUSIONS AND FUTURE WORK

- We used M_L–M_C, which is a depth discriminant, to successfully separate the population of mining blasts (RMEs+QBs) from the group of earthquakes (EQs). The area under the receiver operating characteristic curve (AUC) involving the RMEs and EQs is 0.98, indicating a very effective discriminant.
- Using measured *Sg* amplitudes and a parameterization that linearized the equation relating the observed amplitudes with the source, distance-correction, and site terms, we inverted for each of those terms in three frequency bands (10–15 Hz, 15–20 Hz, and 20–30 Hz).
- Using the isolated source excitation terms, we designed a discriminant that is based on the difference in frequency contents between the mining blasts and earthquakes. The AUC for *Sg* low-to-high frequency ratio ranges from 0.80 to 0.92, with the largest value associated with *Sg*(10–15 Hz)/*Sg*(20–30 Hz).
- We are in the process of designing other discriminants that are effective at these local distances. We will combine two or more discriminants to improve classification power.

ACKNOWLEDGMENTS

Sandia National Laboratories is a multimission laboratory managed and operated by National Technology and Engineering Solutions of Sandia, LLC, a wholly owned subsidiary of Honeywell International, Inc., for the U.S. Department of Energy's National Nuclear Security Administration under contract DE-NA-0003525. The views expressed in the article do not necessarily represent the views of the U.S. Department of Energy or the United States Government. This research was funded by the National Nuclear Security Administration, Defense Nuclear Nonproliferation Research and Development (NNSA DNN R&D). The authors acknowledge important interdisciplinary collaboration with scientists and engineers from LANL, LLNL, MSTS, PNNL, and SNL.

Sandia National Laboratories is a multimission laboratory managed and operated by National Technology & Engineering Solutions of Sandia, LLC, a wholly owned subsidiary of Honeywell International Inc., for the U.S. Department of Energy's National Nuclear Security Administration under contract DE-NA0003525.